Journal of Visualization, Vol. 6, No. 3 (2003) 293-302

Nanoparticle Coagulation in a Temporal Mixing Layer Mean and Size-selected Images

Modem, S.*[1] and Garrick, S. C.*[2]

*1 Graduate Research Assistant, Department of Mechanical Engineering, University of Minnesota, Minneapolis, MN 55455, USA.
*2 Assistant Professor, Department of Mechanical Engineering, University of Minnesota, Minneapolis, MN 55455, USA.

Received 15 January 2002
Revised 5 December 2002

Abstract : Direct numerical simulation of nanoparticle coagulation in a two-dimensional mixing layer is performed. A sectional model is used to discretize the particulate field resulting in a set of coupled non-linear partial differential equations each representing the concentration of particles of a particular size. The advantage of this approach is that it provides a robust mathematical framework for considering the particulate field as a function of space, time, and size with no *a priori* assumptions. The spatio-temporal evolution of the particulate field is visualized via the mean particle diameter and also in a size-specific manner.

Keywords : Nanoparticles, Coagulation, Synthesis, Mixing layer, Direct numerical simulation, General dynamic equation, Sectional method.

1. Introduction

Nanoparticles play an integral role in a wide variety of physical/chemical phenomena and processes. These include but are not restricted to soot formation and growth and the synthesis of nanostructured materials (nanoparticles and coatings). Nanostructured materials are expected to play an increasingly significant role in many major industries in the new millennium (Dagani, 2000). Vapor-phase methodologies are one of the favored processes for the production of nanoparticles because of chemical purity and cost considerations (Pratsinis, 1998; Wooldridge, 1998). Optimizing the production of nanoparticles through the use of modeling and simulation of aerosol processes could translate into reduced cost and nanoparticles with more desirable morphologies and characteristics.

There are several approaches to the modeling and simulation of aerosols. Sectional methods which discretize the particulate phase in size-space are advantageous in that they do not impose any constraints on the nature of the particle size distribution (Gelbard *et al.*, 1980; Gelbard and Seinfeld, 1980; Biswas *et al.*, 1997). They have also been extended to two dimensions to obtain the evolution of both particle size and shape during gas phase production of nanopowders (Xiong and Pratsinis, 1993). However, because of the computational cost, most applications of sectional

methods have been restricted to reduced dimensions and Reynolds-averaged Navier-Stokes (RANS) simulations. Pyykonen and Jokiniemi (2000) employed a sectional method in conjunction with a RANS solver to simulate aerosol formation via nucleation, condensation and coagulation. However, the results obtained were for a steady-state and diffusion was neglected in the axial-direction. As a result, the effects of unsteady hydrodynamics, the underlying turbulence models and axial transport could not be determined.

In this work, direct numerical simulation (DNS) of a coagulating aerosol in a two-dimensional, incompressible, isothermal mixing layer is performed. The spatio-temporal evolution of the particle field is obtained via a sectional model. The use of DNS in conjunction with the sectional model facilitates the capture of the underlying physics in a time-accurate manner (Givi, 1989). This work is unique in that the particle field is obtained as a function of space, time and size without neglect of transport while resolving all of the relevant length and time scales.

2. Formulation

The flows under consideration are two-dimensional, isothermal, incompressible flows and are governed by the conservation of mass and momentum equations:

$$\frac{\partial u_j}{\partial x_j} = 0, \tag{1}$$

$$\frac{\partial u_i}{\partial t} + \frac{\partial u_i u_j}{\partial x_j} = -\frac{1}{\rho}\frac{\partial p}{\partial x_i} + \nu \frac{\partial^2 u_i}{\partial x_j \partial x_j}, \tag{2}$$

where u_i is the fluid velocity in the i direction, ρ is the fluid density, p is the pressure and ν is the kinematic viscosity.

The transport of nanoscale particles dispersed throughout the fluid is governed by the aerosol general dynamic equation (GDE). The GDE describes particle dynamics under the influence of various physical and chemical phenomena: convection, diffusion, coagulation, surface growth, nucleation, and other internal/external forces. Using a sectional model (Gelbhard and Seinfeld, 1980), the GDE is written in discrete form as a population balance on each cluster or particle size. The sectional model is advantageous in that there are no *a priori* assumptions regarding the particle size distribution. It therefore does not suffer from the severe constraints of other methodologies (Zachariah and Semerjian, 1989; Pratsinis and Kim, 1989). The sectional model effectively divides the particle size distribution into "bins." Instead of solving the GDE, we solve a set of N_s coupled equations, where N_s is the number of sections. This representation facilitates the capture of the underlying fluid-particle interactions. In adopting this framework the general transport equation for the concentration of particles is given by

$$\frac{\partial Q_k}{\partial t} + \frac{\partial Q_k u_j}{\partial x_j} = \frac{\partial}{\partial x_j}\left(D_Q \frac{\partial Q_k}{\partial x_j} \right) + \omega_k, \tag{3}$$

where Q_k, $k=1,2,\ldots N_s$, is the number concentration of particles in the k-th section and D_Q is the diffusion coefficient given by

$$D_Q = k_b T \frac{C_c}{3\pi\mu d_p}, \tag{4}$$

where k_b is the Boltzmann constant, T is the fluid temperature, C_c is the Cunningham correction factor, μ is the viscosity and d_p is the particle diameter (Fuchs, 1964; Matsoukas and Friedlander, 1991). The source term ω_k represents the effect of particle-particle collisions leading to particle coagulation. Assuming a brownian collision frequency, the source term is given by

$$\omega_k = \frac{1}{2}\sum_{i=1}^{N_s}\sum_{j=1}^{N_s}\beta_{ij}\chi_{ijk}Q_iQ_j - \sum_{i=1}^{N_s}\beta_{ik}Q_iQ_k\,, \tag{5}$$

where

$$\beta_{ij} = \left(\frac{3}{4\pi}\right)^{\frac{1}{6}}\left(\frac{6k_bT}{\rho_p}\right)^{\frac{1}{2}}\left(\frac{1}{v_i}+\frac{1}{v_j}\right)^{\frac{1}{2}}\left(v_i^{\frac{1}{3}}+v_j^{\frac{1}{3}}\right)^2 \tag{6}$$

and

$$\chi_{ijk} = \begin{cases} \dfrac{v_{k+1}-\left(v_i+v_j\right)}{v_{k+1}-v_k} & \text{if} \quad v_k \le v_i+v_j \le v_{k+1} \\ \dfrac{\left(v_i+v_j\right)-v_{k-1}}{v_k-v_{k-1}} & \text{if} \quad v_{k-1} \le v_i+v_j \le v_k \\ 0 & \text{otherwise,} \end{cases} \tag{7}$$

where v_i is the volume of a particle in section i, ρ_p is the particle density and β_{ij} is the collision frequency. The collision frequency β_{ij} represents the probability with which particles in section i and section j collide. The derivation of this form, Eq. (6), comes from the kinetic theory of gases (the particle diameters are smaller than the mean free path of the carrier gas as is true for gas molecules) under the assumption that inter-particle forces are insignificant (*e.g.* electrostatic, van der Waals). Our studies are confined to particles in the free molecule regime where the Knudsen number is greater than unity, i.e. $Kn > 1$. This implies that mean free paths over $400\ nm$ are expected and growth of aerosols for sizes below this value can be based on one form of the collision frequency function β_{ij}. The collision frequency considers only Brownian collisions as the effects of turbulent shear in the coagulation of nanoparticles is negligible (Prupacher and Klett, 1978). The Kolmogorov length scales are much larger than those associated with the nanoparticles. An additional simplification in working with small particle sizes is that the Stokes number is sufficiently small, which implies that particle velocity slip can be neglected and we can treat the whole problem as a single phase flow, i.e. particle inertial effects can be ignored. Implicit in this formulation of β_{ij} is the assumption that all particles are spherical. This implies that coalescence processes are effectively instantaneous. The sectional method is discretized in size space such that the volume of particles in two successive sections is doubled, i.e. $v_i = 2\times v_{i-1}$. Because of the logarithmic spacing of particle sizes, a collision of two particles typically results in a size that lies between sections. The operator χ_{ijk} "splits" such particles into neighboring sections in such a way that the first two moments of the particle size distribution – the particle mass and particle number – are preserved.

3. Results

3.1 Flow Configuration and Numerical Specification

The flow considered is a two-dimensional, incompressible, temporal mixing layer. A mixing layer is formed when two co-flowing streams with different velocities meet at the trailing edge of a splitter plate. The temporal evolution is considered by attaching a reference frame to the fluid as it travels downstream. The space coordinates are $\boldsymbol{x} = [x,y]$ where x is the streamwise direction, and y is the cross-stream direction. The Reynolds number, based on the initial vorticity thickness, δ, and the velocity difference between the two streams, $\Delta U = (U_1 - U_2)/2$, is $Re_\delta = \Delta U \delta / \nu = 200$. The flow is dominated by large-scale coherent structures, the formation of which are expedited by the addition low-amplitude perturbations. The length in the streamwise direction is twice the wavelength of the most unstable mode to allow for the roll-up and subsequent pairing of two vortices. In this study, the lower stream is initially laden with particles of diameter d_p=*1nm*, as shown in Fig. 1. The flow is isothermal at a temperature of *T=300 K*; therefore, no thermophoretic effects are present. Thermophoresis poses no additional modeling or computational difficulties and has been included in a previous work (Modem *et al.,* 2002). A total of ten sections are solved, i.e. N_s=*10*. This facilitates the solution of particles covering a range of four orders of magnitude in volume, or particles ranging from 1 to 8 nanometers in diameter. The initial volume fraction, or the ratio of the volume occupied by the particles to that occupied by the gas is $\Phi = 9.5 \times 10^{-8}$.

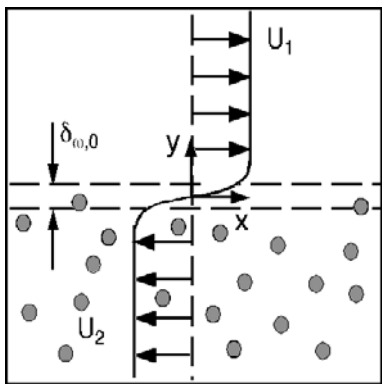

Fig. 1. Flow configuration and initial particle distribution.

The computational domain is covered by a mesh consisting of *1500* x *1500* points in the x and y directions. The large number of grid points is necessary because of the diffusivity of the larger particles. The resolution was arrived at by comparing results at successively higher resolutions. When the solutions were found to vary by less than 0.001%, the simulation was deemed to be grid-independent. Periodic boundary conditions are used in the streamwise x-direction, while the freestream or zero-derivative conditions are imposed in the cross-stream y-direction. The governing transport equations are solved using a hybrid MacCormack based compact difference scheme (MacCormack, 1969; Carpenter, 1990). The numerical scheme used is based on the one-parameter family of dissipative two-four schemes. The accuracy of the scheme is second order in time and fourth order in space. All calculations are performed on a rectangular uniformly spaced grid. The exact details of the numerical schemes employed in this study are not given here but a catalog of these schemes, and others, is readily available (Carpenter, 1990; Kennedy and Carpenter, 1994). All simulations were performed until the size of the eddies approached the size of the computational domain, a non-dimensional time of $t^* = t/(\delta_\omega / U_o) = 14.25$.

3.2 Particle field

The lower stream is initially populated by d_p=*1 nm* diameter particles, while the upper stream is initially particle free. As the flow evolves, the particles in the particle-laden stream collide, coagulate, grow in size and move from lower-numbered sections to higher-numbered sections. In addition to undergoing coagulation, particles are also dispersed from the particle-laden stream to the particle-free stream as the eddy evolves. The temporal evolution of the d_p=*5 nm* diameter (section k=*8*) particles is shown in Fig. 2. Instantaneous snapshots of the normalized particle concentration, Q_8*, are shown for four times. All values of particle concentrations are normalized by the initial number of particles in the lower, or particle-laden, stream, Q_{1o}, i.e. Q_k*= Q_k/Q_{1o}. The images reveal that between t*=*0* and t*=*12.3*, the number of particles in the particle-laden stream increases with time. Figure 2 also reveals a deficit of d_p=*5 nm* particles in the eddy core, implying that the particles are growing more slowly in this region. As the eddy "rolls up," the particle-laden stream engulfs the particle-free fluid. This dilutes or reduces the particle concentration resulting in a decreased growth rate. Additionally, particles move across the concentration gradient due to the effects of diffusion. This reduces the population of the smaller particles and acts to reduce the growth rate in the neighborhood of the interface. As the particles become larger their diffusion coefficient becomes smaller and gradients in their concentration are maintained. This is evident in the striations observed in Fig. 2(d).

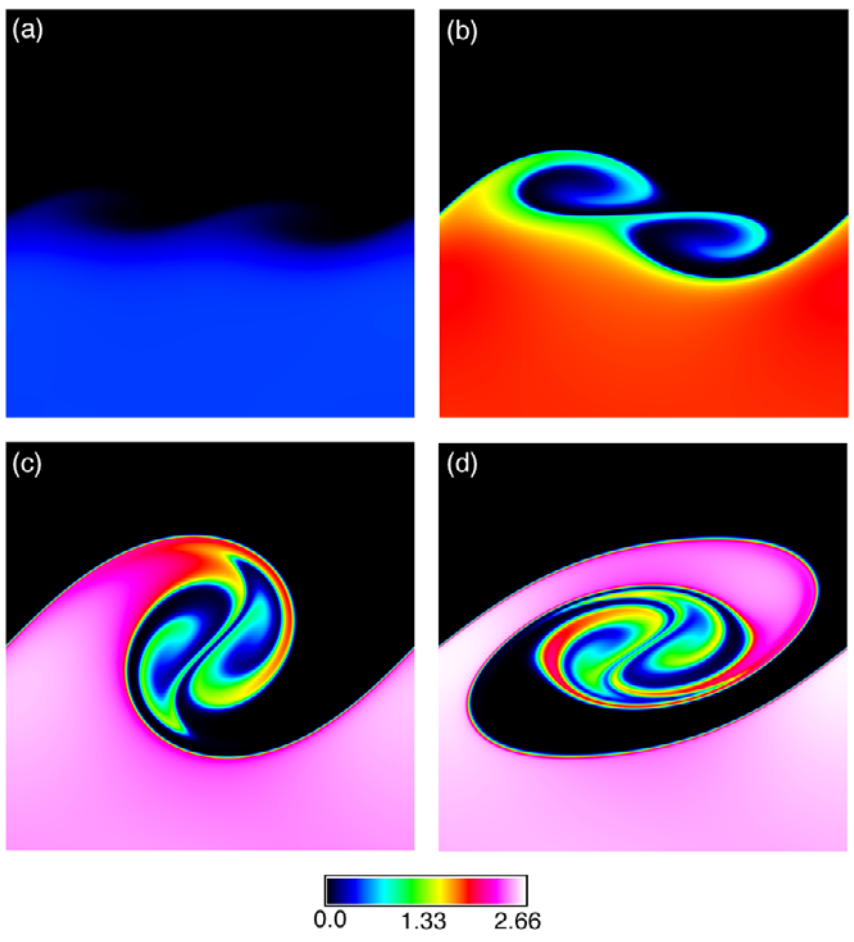

Fig. 2. Instantaneous d_p=*5 nm* particle concentration contours, $Q^*_8 \times 10^3$.
(a) t*=*2.74,* (b) t*=*6.01,* (c) t*=*9.13,* (d) t*=*12.3*.

The spatial distribution, and the extent to which particles of different sizes are segregated, may be observed by considering the concentration of particle of different sizes at one instant in time. Figure 3 shows the instantaneous contours of the concentration of particles sized d_p=*1 nm,* d_p=*2 nm,* d_p=*4 nm, and* d_p=*8 nm* (sections *k=1, 4, 7* and *10)* at time *t*=9.13*. This view illustrates the structure of the particulate field as a function of space and size. Figure 3(a) reveals that at time *t*=9.13*, the highest concentration of d_p=*1 nm* particles is found in a region of the fluid which was initially particle free, located to the right of the eddy. The d_p=*1 nm* particles in the particle-laden stream have coagulated, increased their size, and moved out of section *k=1.* Even inside the eddy core few particles remain. A small number – 0.3% of the initial concentration – of Q_1 particles exists in a thin band separating the two streams. Figure 3(b) reveals that at the same time, the peak concentration of d_p=*2 nm* particles in the eddy-core is twice that in the particle-laden stream. Figure 3(c) shows that the highest concentration of d_p=*4 nm* particles is found in the freestream, while between *50%* and *90%* of the peak concentration may be found in the eddy core. Figure 3(d) reveals that the core is virtually devoid of d_p=*8 nm* particles. Though this view represents only one instant in time, the images in Fig. 3 suggest reduced growth rates in the eddy core. Additionally, these images shed light on the nature of the particle-particle interactions. For example, Q_1-Q_7 collisions occur predominantly near the interface of the two streams while Q_4-Q_7 collisions occur predominantly in the eddy-core.

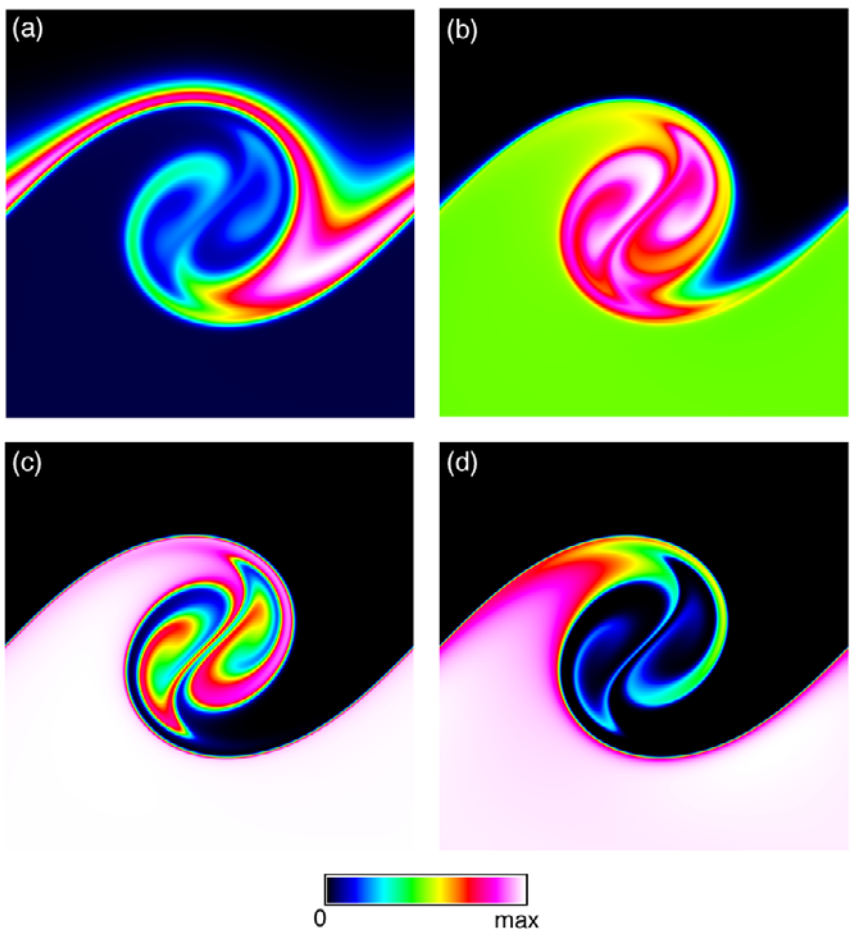

Fig. 3. Instantaneous particle concentration contours at t* = 9.13.
(a) d_p=*1 nm,* (b) d_p=*2 nm,* (c) d_p=*4 nm,* (d) d_p=*8 nm*.

The temporal evolution of mean particle diameter is portrayed in Fig. 4. This diameter is computed from the mean particle volume given by

$$\bar{v} = \frac{\sum_{k=1}^{N_s} Q_k v_k}{\sum_{k=1}^{N_s} Q_k} \tag{8}$$

and $\bar{d} = (6\bar{v}/\pi)^{1/3}$. The figure shows that of the particle-containing regions, the mean diameter is maximum in the particle laden stream and is a minimum in the core of the eddy. The spread of the mean diameter into the initially particle-free stream, seen as the vortex develops in time, reflects the dispersion of particles into the particle-free stream and their subsequent coagulation. The mean diameter is greatest in the particle-laden stream due to the higher concentration of larger particles. Near the interface, dispersion and transport act to mix the two streams, macroscopically and microscopically, thereby reducing the local particle number concentration. It is evident from Fig. 4(c) that the smallest particles are found near the initially particle-free stream in the periphery of the eddy (also observed in Fig. 3(c)). The mean diameter contours shown in Fig. 4 also reveal that as time increases, the striations in the eddy core become both thin and more folded. This is due to the nature of the diffusion coefficient, D_Q, (Eq. (4)). The diffusion of each particle is proportional to the reciprocal of the square of its diameter, d_p (an additional $1/d_p$ is contained within C_c). Therefore, particles diffuse less as they become larger, resulting in a reduced striation thickness (Ottino, 1989).

The evolution of the geometric standard deviation σ_g is shown in Fig. 5. The geometric standard deviation is a measure of the width of the particle size distribution and is given by

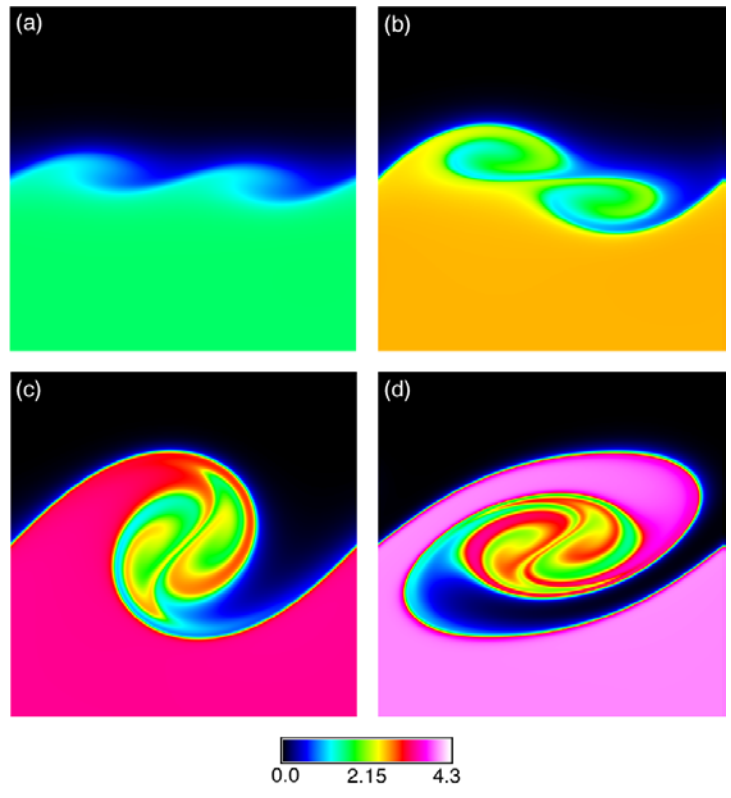

Fig. 4. Instantaneous contours of mean particle diameter, d_p (*nm*).
(a) $t^*=2.74$, (b) $t^*=6.01$, (c) $t^*=9.13$, (d) $t^*=12.3$.

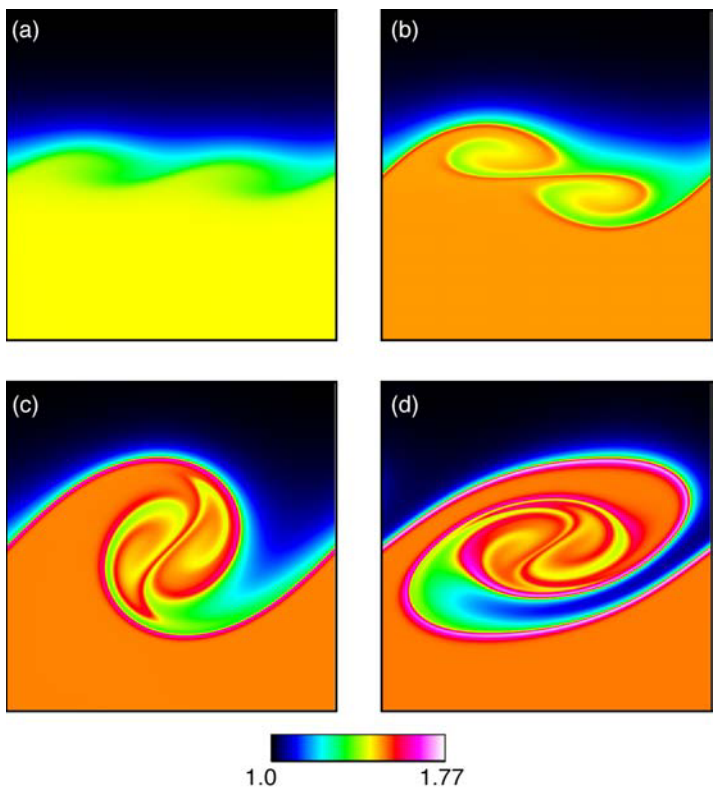

Fig. 5. Instantaneous contours of geometric standard deviation σ_g.
(a) *t*=2.74,* (b) *t*=6.01,* (c) *t*=9.13,* (d) *t*=12.3.*

$$\log^2 \sigma_g = \frac{\sum_{k=1}^{N_s} Q_k (\log d_p - \overline{\log d_p})^2}{\sum_{k=1}^{N_s} Q_k} \tag{9}$$

where

$$\overline{\log d_p} = \frac{\sum_{k=1}^{N_s} Q_k \log d_p}{\sum_{k=1}^{N_s} Q_k} \tag{10}$$

As coagulating aerosols reach the self-preserving limit, σ_g approaches a fixed value. Using a sectional method in which the volume of successive sections double, the limiting value is σ_g*=1.5* (Pratsinis and Kim, 1989; Pykonnen and Jokiniemi, 2000). The images reveal that by time *t*=6.01* (Fig. 3(b)), the self-preserving limit is reached in the particle-laden stream. The images also show that the largest values of the geometric standard deviation are found near the interface of the two streams, indicating that a wider variety of particles are found in this region, while the eddy-core is characterized by values at or less than σ_g*=1.5*. This implies that the effects of transport are strongest in the shear region.

4. Conclusions

DNS of nanoparticle coagulation in an incompressible temporal mixing layer has been performed. A sectional method was employed to represent the particle field in an eulerian manner. One stream was particle free while the other stream was laden with 1 nanometer diameter particles. Simulations were performed at one Reynolds number and one volume fraction. Both mean size, and size-selected images of the particle field were presented as a function of space and time.

The images revealed that the largest particles were found in the homogeneous region of the particle-laden stream and the growth rate was reduced within the core of the eddy. Smaller particles were found in a thin region near the interface of the two streams. The images also illustrated the differential diffusion nature of the particle field as the concentration contour striation thicknesses decreased as the particles grew larger, illustrating the need for a large number of grid points. One significant contribution of this work is preferential concentration or segregation of different size particles. This is the result of the non-linear interactions between diffusion and coagulation which can greatly alter nanoparticle growth rates in turbulent flows. Additionally, the simulation shows larger-than-self-preserving values of the geometric standard deviation. This further elucidates the effects of spatial gradients in nanoparticle coagulation. In summary, the method provides a robust mathematical framework for the inclusion of other particle processes such as nucleation, evaporation/condensation, and surface chemistry along with a dataset from which the effects of turbulence on the nanoparticle coagulation maybe be investigated.

Acknowledgements

This work was supported in part by the National Science Foundation under grant ACI-9982274. Computing resources were provided by the Minnesota Supercomputing Institute and Digital Technology Center.

References

Biswas, P., Wu, C. Y., Zachariah, M. R. and McMillen, B. K., In Situ Characterization of Vapor Phase Growth of Iron Oxide-Silica Nanocomposite; Part II: Comparison of a Discrete-Sectional Model Predictions to Experimental Data, Journal of Material Research, 12-3 (1997) 714-723.

Carpenter, M. H., A High-Order Compact Numerical Algorithm for Supersonic Flows, In Morton, K. W., editor, Twelfth International Conference on Numerical Methods in Fluid Dynamics, Lecture Notes in Physics, 371 (1990), 254-258, Springer-Verlag, New York, NY.

Dagani, R., NASA Goes Nano, Chemical Engineering News, (2000).

Garrick, S. C., Lehtinen, K. E. J and Zachariah, M. R., Modeling and Simulation of Nanoparticle Coagulation in High Reynolds Number Incompressible Flows, proc. Joint US Sections Meeting of the Combustion Institute, (Oakland, CA), (2001).

Gelbard, F., Tambour, R. and Seinfeld, J. H., Sectional Representations for Simulating Aerosol Dynamics, Journal of Colloid and Interface Science, 76-2:541-556.

Gelbard, F. and Seinfeld, J. H., Simulation of Multi-component Aerosol Dynamics, Journal of Colloid and Interface Science, 78-2 (1980), 485-501.

Fuchs, N. A., The Mechanics of Aerosols, Pergamom, Toronto, CA, (1964).

Givi, P., Model Free Simulations of Turbulent Reactive Flows, Progress in Energy Combustion Science, 15 (1989), 1-107.

Kennedy, C. A. and Carpenter, M. H., Several New Numerical Methods For Compressible Shear-Layer Simulations, Applied Numerical Mathematics, 14 (1994), 397-433.

MacCormack, R. W., The Effect of Viscosity in Hypervelocity Impact Catering, AIAA Paper 69-354 (1969).

Matsoukas, T. and Friedlander, S. K., Dynamics of Aerosol Agglomerate Formation, Journal of Colloid and Interface Science, 146-2 (1991), 495-506.

Modem, S., Garrick, S.C., Lehtinen, K. E. J., and Zachariah, M. R., Direct Numerical Simulation of Nanoparticle Coagulationi in Temporal Mixing Layers, proc. the (29th) Int. Symposium on Combustion, (*in press*).

Ottino, J. M., The Kinematics of Mixing: Stretching, Chaos, and Transport, Cambridge University Press, Cambridge, UK, (1989).

Pratsinis, S. E., Flame Aerosol Synthesis of Ceramic Powders, Progress in Energy Combustion Science, 24 (1998) 197-219.

Pratsinis, S. E. and Kim, K.S., Particle Coagulation, Diffusion, and Thermophoresis in Laminar Flows, Journal of Aerosol

Science, 20 (1989), 101-111.
Prupacher, H. R. and Klett, J. D., Microphysics of Clouds and Precipitation, Reidel, Dordrecht, Netherlands, (1978).
Pyykonen, J. and Jokiniemi, J., Computational Fluid Dynamics Based Sectional Aerosol Modelling Schemes, Journal of Aerosol Science, 31 (2000), 531-550.
Wooldridge, M. S., Gas Phase Combustion Synthesis of Particles, Progress in Energy Combustion Science, 24 (1998) 197-219.
Xiong, Y. and Pratsinis, S. E. Formation of Agglomerate Particles by Coagulation and Sintering, Part-I. A 2-d Solution of the Population Balance Equation, Journal of Aerosol Science, 24 (1993), 283-300.
Zachariah, M. and Semerjian, H., Simulation of Ceramic Particle Formation: Comparison With In-Situ Measurements, American Institute of Chemical Engineering Journal, 35 (1989), 2003-2012.

Author Profile

Sean Garrick: He is the Nelson Assistant Professor of Mechanical Engineering at the University of Minnesota – Twin Cities. Professor Garrick obtained his Ph.D. in Mechanical Engineering at the State University of New York at Buffalo in 1998. His research interests include turbulent reacting flows, stochastic processes, aerosols, large eddy simulation, and heat transfer.

Sriswetha Modem: She is a Ph.D. candidate in the department of Mechanical Engineering at the University of Minnesota – Twin Cities. Ms. Modem received her M.S. degree in 2001 from the Department of Mechanical Engineering at the University of Minnesota – Twin Cities. Her research interests include computational fluid dynamics, reacting flows, mixing layers, and jets.